CHEMMEDCHEM

DOI: 10.1002/cmdc.201100168

Design, Synthesis, and Biological Activity of Urea Derivatives as Anaplastic Lymphoma Kinase Inhibitors

Gustav Boije af Gennäs,[a] Luca Mologni,[b] Shaheen Ahmed,[c] Mohanathas Rajaratnam,[a] Oriano Marin,[d] Niko Lindholm,[a] Michela Viltadi,[b] Carlo Gambacorti-Passerini,*[b] Leonardo Scapozza,*[c] and Jari Yli-Kauhaluoma*[a]

In anaplastic large-cell lymphomas, chromosomal translocations involving the kinase domain of anaplastic lymphoma kinase (ALK), generally fused to the 5′ part of the nucleophosmin gene, produce highly oncogenic ALK fusion proteins that deregulate cell cycle, apoptosis, and differentiation in these cells. Other fusion oncoproteins involving ALK, such as echinoderm microtubule-associated protein-like 4-ALK, were recently found in patients with non-small-cell lung, breast, and colorectal cancers. Recent research has focused on the development of inhibitors for targeted therapy of these ALK-positive tumors. Because kinase inhibitors that target the inactive conformation are thought to be more specific than ATP-targeted inhibitors, we investigated the possibility of using two known inhibitors, doramapimod and sorafenib, which target inactive kinases, to design new urea derivatives as ALK inhibitors. We generated a homology model of ALK in its inactive conformation complexed with doramapimod or sorafenib in its active site. The results elucidated why doramapimod is a weak inhibitor and why sorafenib does not inhibit ALK. Virtual screening of commercially available compounds using the homology model of ALK yielded candidate inhibitors, which were tested using biochemical assays. Herein we present the design, synthesis, biological activity, and structure–activity relationships of a novel series of urea compounds as potent ALK inhibitors. Some compounds showed inhibition of purified ALK in the high nanomolar range and selective antiproliferative activity on ALK-positive cells.

Introduction

Anaplastic lymphoma kinase (ALK) is a receptor tyrosine kinase (RTK) that is composed of an extracellular ligand binding domain, a putative transmembrane domain, and a cytoplasmic kinase domain.[1] Among the RTKs, the extracellular domain of ALK is most similar to that of leukocyte tyrosine kinase (LTK),[2] which is a member of the superfamily of insulin receptors. ALK plays an important role in the development of the central and peripheral nervous system.[3] However, ALK can be aberrantly activated as a result of the (2;5)(p23;q35) chromosomal translocation in anaplastic large-cell lymphomas (ALCLs).[4,5] In most cases, the translocation causes fusion of the intracellular catalytic domain of ALK with the oligomerization domain of nucleophosmin (NPM). The resulting NPM–ALK fusion product has constitutive kinase activity and is highly oncogenic.[6] Several additional fusion partners that have dimerization domains have been described.[7] Oncogenic mutants or fusion variants of ALK have also been identified in neuroblastomas, inflammatory myofibroblastic tumors and diffuse large B-cell lymphoma.[1] Furthermore, the echinoderm microtubule-associated protein-like 4 (EML4)–ALK fusion gene was recently discovered to be expressed in a subset of non-small-cell lung cancers (NSCLCs), breast and colorectal cancers.[8,9]

Sixty to eighty percent of ALCLs are ALK-positive, and 70–80% of ALK-positive ALCLs express the NPM–ALK fusion protein.[10] ALK-positive ALCL tends to affect children and favor males. Primary systemic ALCL has a peak incidence in children or young adults, accounting for ~20–30% of non-Hodgkin lymphomas (NHL) in this age group. Although ALK-positive ALCL patients are responsive to cytotoxic drugs, relapses occur frequently and bear a dismal prognosis.

There are several reasons for the increase in ALK research for the treatment of ALCLs. Importantly, ALK expression is restricted to rare scattered neural cells.[11] Despite the role of ALK in

[a] G. Boije af Gennäs,[+] Dr. M. Rajaratnam, N. Lindholm, Prof. J. Yli-Kauhaluoma
Division of Pharmaceutical Chemistry
Faculty of Pharmacy, University of Helsinki
P.O. Box 56 (Viikinkaari 5E), 00014 Helsinki (Finland)
Fax: (+358) 9-191-59556
E-mail: jari.yli-kauhaluoma@helsinki.fi

[b] Dr. L. Mologni,[+] M. Viltadi, Prof. C. Gambacorti-Passerini
Department of Clinical Medicine and Prevention
University of Milano-Bicocca, Via Cadore 48, 20052 Monza (Italy)
Fax: (+39) 039-233-3539
E-mail: carlo.gambacorti@unimib.it

[c] Dr. S. Ahmed,[+] Prof. L. Scapozza
Group of Pharmaceutical Biochemistry
School of Pharmaceutical Sciences, University of Geneva
Quai Ernest-Ansermet 30, 1211 Genève 4 (Switzerland)
Fax: (+41) 22-379-3360
E-mail: leonardo.scapozza@unige.ch

[d] Prof. O. Marin
Peptide Facility, CRIBI-Biotechnology Centre
University of Padova, Viale Colombo 3, 35131 Padova (Italy)

[+] These authors contributed equally to this work.

Supporting information for this article is available on the WWW under http://dx.doi.org/10.1002/cmdc.201100168.

development and expression patterns, ALK-deficient mice appear normal and display no visible tissue abnormalities.[12] Therefore, minimal side effects result from ALK inhibition. In addition, children show more ALK-positive ALCLs than adults, encouraging the search for safe treatments that will be effective for long-term use. Another important reason for research of ALK is that immunological responses elicited against ALK will probably not produce a relevant autoimmune disease. Finally, new inhibitors are needed to combat mutations in the oncogene. For instance, the c-Met/ALK inhibitor crizotinib is the first agent in phase III clinical trials that selectively targets EML4–ALK in NSCLC.[13]

The majority of RTK inhibitors target the highly conserved ATP binding pocket[14] and have a high risk of producing side effects.[15] Therefore, to obtain kinase specificity, inhibitors that also bind to less conserved residues outside the ATP binding pocket are desirable.[16] In addition, inhibitors that target the inactive conformation of kinases would have increased specificity.[17,18]

ALK is a clinically relevant target, and there is a need for new therapeutics for the treatment of ALK-positive tumors. Drug resistance, nonspecific binding by ATP-competitive inhibitors, and poor life expectancy for the patients involved are the primary reasons we sought to develop novel ALK-targeted inhibitors. Herein we present a novel series of urea compounds as potent ALK inhibitors, some of which show activity in both purified ALK and cellular assays.

Results and Discussion

Design of urea compounds as potent NPM–ALK inhibitors

A model of ALK corresponding to the inactive conformation of the catalytic site was generated using mouse c-Abl (PDB IDs: 1IEP, 1OPJ; 34% identity with ALK amino acid sequence) and human insulin receptor (PDB ID: 1IRK; 40% identity with ALK) as templates. The model was built before X-ray crystal structures of ALK were available; however, the overall structure is very close to the published one, the only difference being that the X-ray structure shows a DFG-Asp-in conformation, typical of an active conformation.[19,20]

The ZINC database,[21] a free database of commercially available compounds, was virtually screened by using our homology model of ALK (see Experimental Section for details). This initial screen yielded a series of potential ALK inhibitors. Among the top-ranked hits, several urea-derived molecules were identified, and they were chosen as starting points for the development of derivatives with increased potency and specificity, as there is structural data available on how related compounds from this class (such as sorafenib and doramapimod) bind to other kinases (MAP kinase in particular). Our docking protocol yielded a very similar binding mode for the ureas in the ALK inactive model, as compared with available X-ray data with protein kinase–urea inhibitor complexes. Urea-based compounds have previously been described as potent kinase inhibitors.[22–24]

Sorafenib, a multi-kinase inhibitor that targets VEGFR, PDGFR, KIT, FLT-3 and RET receptor tyrosine kinases, MAP kinases, and Raf kinases, was approved in 2006 for the treatment of advanced renal cell carcinoma (primary kidney cancer). Doramapimod (BIRB-796) is a potent inhibitor of MAP kinases with an IC_{50} value of 63 nM. It also inhibits other kinases, such as Abl kinase, with considerable potency. This compound was tested in phase II clinical trials for patients of rheumatic arthritis, Crohn's disease, and psoriasis,[25] but was withdrawn owing to liver toxicity.[26] In this study, a novel series of urea compounds, which were derived from sorafenib and doramapimod as well as hits from virtual screening of the ZINC database, were designed, synthesized, and tested for ALK inhibition.

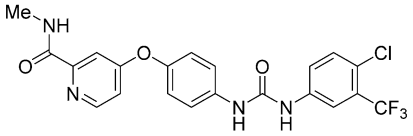

Sorafenib

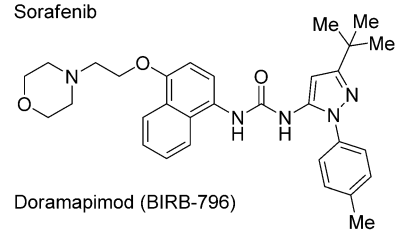

Doramapimod (BIRB-796)

Doramapimod is a weak inhibitor of ALK (IC_{50} = 45 μM), whereas sorafenib does not inhibit ALK and only weakly inhibits Abl (IC_{50} = 25 μM), but is a potent inhibitor of RET (IC_{50} = 6 nM).[17] Doramapimod and sorafenib bind the inactive conformation (DFG-Asp-out) of p38 MAP kinase (Figure 1A and Figure 2B).[27,28] Sorafenib also binds the inactive conformation of B-Raf.[29] To elucidate the activity of these inhibitors toward ALK, doramapimod and sorafenib were docked into the active site of a homology model of ALK in its inactive (DFG-Asp-out) conformation. Superposition of the model of inactive ALK with the crystal structures of ALK containing NVP-TAE684 (PDB ID: 2XB7)[22] and missing the activation loop yielded an overall root mean square deviation (RMSD) of 0.68 Å, indicating very good agreement between the model and the recently solved crystal structures. The primary difference between the active site of the model and that of the crystal structure is the conformation of the DFG motif, which is in the DFG-Asp-in conformation (active) in the X-ray structure and in the inactive DFG-Asp-out conformation in the model. Furthermore, the model and structure differ in the P-loop, which adopts a different conformation depending on the inhibitor bound.[19,20] Figure 1B shows the docking pose of doramapimod bound to inactive ALK superimposed on the X-ray structure of the compound bound to p38 MAP kinase (PDB ID: 1KV2). There are some significant differences in these two binding modes, which may explain why doramapimod is a weak inhibitor of ALK. The bulky gatekeeper residue in ALK (leucine), in contrast to that of p38 MAP kinase (threonine), prevents the naphthyl ring of doramapimod from adopting the same conformation as observed when bound to p38 MAP kinase. Thus, molecular dock-

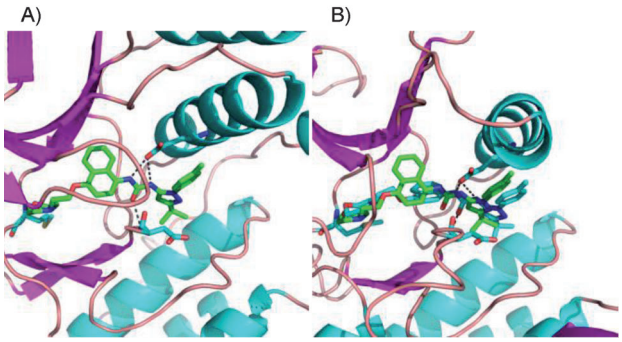

Figure 1. A) Binding mode of doramapimod in the active site of p38 MAP kinase (PDB ID: 1KV2). Doramapimod is shown in sticks with green carbon atoms. Residues E71 of the α-helix C and D186 of the DFG motif as well as M109 of the hinge region are shown as sticks and are colored by atom type. Hydrogen bonds (donor–acceptor distance: 2.8–3.2 Å, angle: 140–180°) are depicted with black dotted lines. B) Doramapimod (sticks, cyan carbon atoms) docked in the active site of inactive ALK showing the necessary flip of the naphthyl moiety. The position of doramapimod in the crystal structure of p38 MAP kinase is superimposed (sticks, green carbon atoms). The residues M259 of the hinge, E227 of the α-helix C and D330 of the DFG motif of ALK are shown as sticks with blue carbon atoms. Hydrogen bonds are depicted with black dotted lines. The 3D structure of p38 MAP kinase (A) and the ALK kinase domain (B) are shown as ribbons with their secondary structures colored as follows: β-strands: magenta, helices: cyan, loops: pink. For the sake of clarity, the gatekeeper residue (L256 for ALK and T106 for p38 MAP kinase) situated behind the naphthyl moiety of the inhibitor is not shown.

ing predicts an approximate 60° tilt of the naphthyl moiety. This tilt causes loss of the hydrogen bond interaction between the morpholino moiety and the hinge region. Furthermore, a slight shift is observed in the urea portion of the molecule, where strong hydrogen bonding that involves the side chain of E71 from α-helix C and the backbone of D168 within the DFG motif is observed in the crystal structure of p38 MAP kinase. These observations may explain why doramapimod is only a weak inhibitor of ALK.

The crystal structure of p38 MAP kinase complexed with sorafenib (PDB ID: 3GCS, Figure 2B) reveals a marked conformational change at the hinge region relative to both the p38 MAP kinase–doramapimod complex (1KV2) and our ALK inactive model (Figure 2A). This conformational change is thought to be essential for the tight hydrophobic interactions of sorafenib with residues V30 and V38 in the p38 MAP kinase active site. However, the modified conformation of the hinge region adopted by p38 MAP kinase in complex with sorafenib would not allow binding of doramapimod because of a clash between the morpholino moiety and the hinge (Figure 2A). The conformation of the ALK hinge region was modeled closer to that of p38 MAP kinase in complex with doramapimod (1KV2) because the conformational change observed in the p38 MAP kinase–sorafenib complex has been rarely observed and might not be possible in ALK due to the different length and amino acid sequence of the hinge region (MAGGD [residues 259–263] for ALK and MGAD [residues 109–112] for p38 MAP kinase; see alignment in Figure 2D). Furthermore, the phenyl ring of sorafenib is in close proximity to the bulky gatekeeper residue of ALK and shows a similar conformational change to the corresponding naphthyl moiety in doramapimod when docked in ALK (Figure 2C) relative to p38 MAP kinase. As for doramapimod, a disrupted hydrogen bonding pattern relative to that of sorafenib in ALK has been observed. This finding suggests an unfavorable strain in the docked poses of doramapimod and sorafenib in ALK. Because sorafenib does not inhibit ALK, we hypothesize that ALK is not able to adopt the specific hinge conformation for binding sorafenib. Furthermore, recently solved ALK structures reveal a hinge region conformation very similar to our model (figure S1 in Supporting Information).[19,20] Based on this comparative analysis, the model of the ALK inactive DFG-Asp-out conformation seems to be able to discriminate, at least to some extent, between urea-based binders (doramapimod) and non-binders (sorafenib).

Virtual hits from the in silico screen were further assayed in vitro for inhibition of recombinant ALK and ALK-dependent cell proliferation. Biochemical assays revealed six experimental hits **I**–**VI** as shown in Figure 3. For a direct comparison, ALK inhibitor NVP-TAE684[18] inhibited the isolated enzyme with an IC_{50} value of 60 nM and showed selective anti-NPM–ALK cell proliferation (BaF3-NPM–ALK: IC_{50} = 110 nM; BaF3 parental: IC_{50} = 980 nM) when measured under the same conditions.

These candidates were selected as a backbone for the development of novel urea compounds with improved potency and selectivity toward ALK. Whereas some of the candidate inhibitors **I**–**VI** showed good inhibitory potency with sub-micromolar IC_{50} values in cell-free assays, no inhibitors showed activity at solubility limits in cells. Thus, in addition to improving inhibition of the purified enzyme, one of the major challenges was to gain inhibitor activity and selectivity in cells. From the virtual screening hits, it was apparent that the additional amide bonds of **IV** relative to **III** are not involved in hydrogen bonding to the protein, as these two compounds have very similar IC_{50} values. Therefore, we investigated the possibility of forming hydrogen bonds to the hinge region by changing the substituents on rings 1 and 2 of candidates **I**–**IV** (Figure 3). In addition, we wanted to explore the possibility of forming interactions to the gatekeeper (L256) by adding a hydrophobic substituent at ring 2 in **I** or **III**. Moreover, we designed analogues of candidates **I** and **II** to compare the influence of various substituents on the pyrazolyl ring toward cellular and enzymatic activity. To investigate the aforementioned interactions and the influence of structural modifications on enzymatic and cellular activity, we selected the 1-phenyl-3-(pyrazol-5-yl)urea and 1,3-diphenylurea backbones of candidates **I**–**VI** to design three series of compounds (Tables 1–3).

Synthesis

Candidates **I** and **II** were used in the design of the two first series of compounds (Figure 3, Table 1, and Table 2). Compounds **1**, **7**, **8**, **13**, and **15** were each prepared in a single step with the respective commercially available isocyanates **25**–**28** and pyrazoles **29**–**31** (Scheme 1). For the synthesis of compounds **11** and **12**, pyrazoles **29** and **30**, respectively, were first treated with phosgene, and the resulting isocyanates **32** and **33** were allowed to react with 4-(2-morpholin-4-ylethoxy)phe-

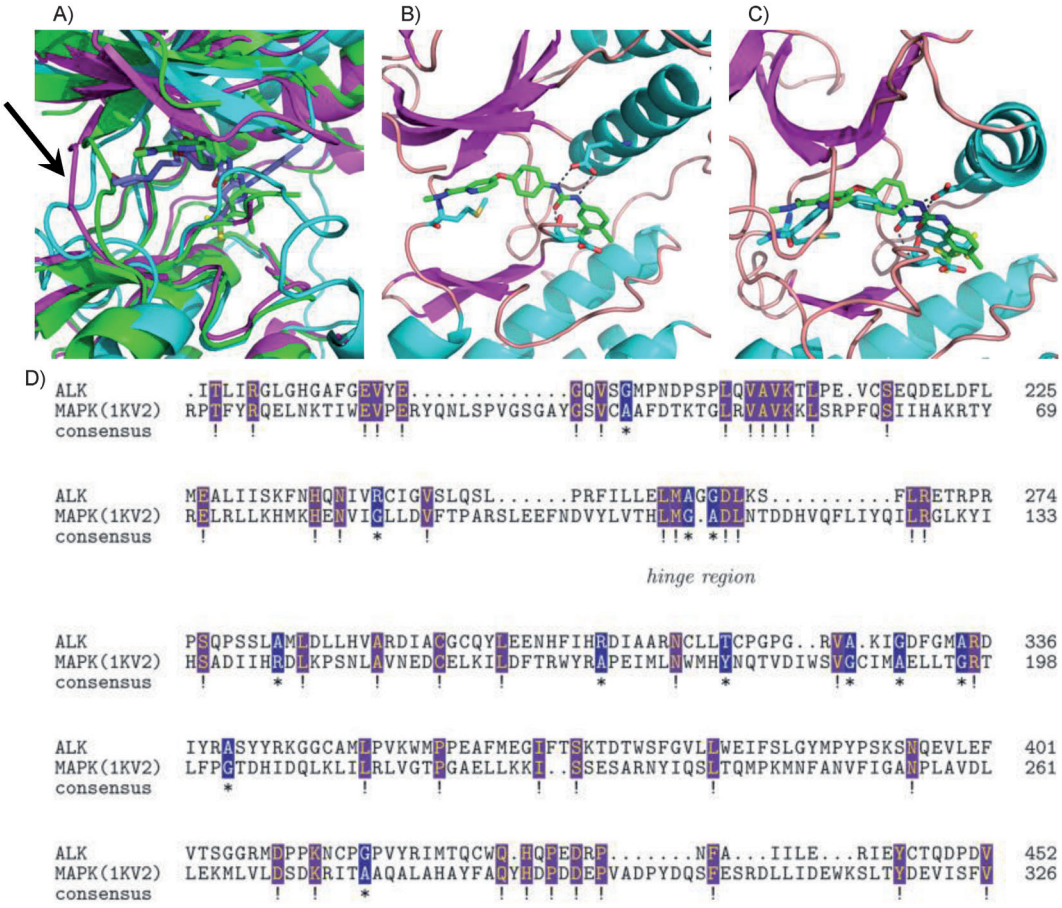

Figure 2. A) Superposition of the ALK inactive conformation (cyan), p38 MAP kinase complexed with doramapimod (magenta, PDB ID: 1KV2) and p38 MAP kinase complexed with sorafenib (green, PDB ID: 3GCS). The crystallographic binding position of sorafenib in the active site of p38 MAP kinase is depicted as sticks with green carbon atoms. The view is rotated by 60° along the *y*-axis relative to Figure 1 A to emphasize the hinge region. The black arrow indicates the various conformations of the hinge region and the clash between doramapimod (sticks, violet carbon atoms) and the hinge region of the sorafenib p38 conformation (green). B) Sorafenib (sticks, green carbon atoms) in the active site of p38 MAP kinase (PDB ID: 3GCS). Residues involved in hydrogen bonding (E71 and D186) and M109 within the hinge region are shown as sticks and colored by atom type. Hydrogen bonds are depicted with black dotted lines. C) Sorafenib (sticks, cyan carbon atoms) docked in the active site of inactive ALK. A crystal structure of sorafenib bound to p38 MAP kinase is superimposed (sticks, green carbons). Hydrogen bonds are depicted with black dotted lines. The same residues as in Figure 1 B (E227, M259, and D330) are shown as sticks. The protein in Figure 2 B,C is shown in Figure 1 A. For the sake of clarity, the gatekeeper is not shown. D) Structural alignment of ALK and p38 MAP kinase domains. Identical and similar residues are indicated with a violet background with yellow and white letters, respectively. The hinge region is denoted.

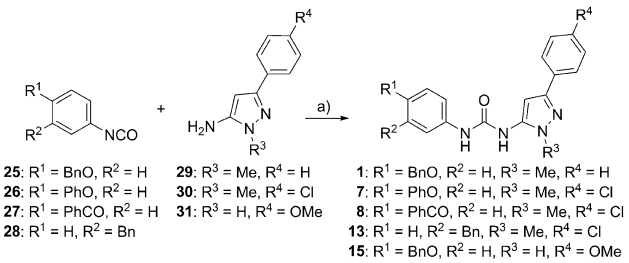

Scheme 1. *Reagents and conditions*: a) THF, RT, 12–15 h, 65–90% (**1**, **7**, **8**, **13**) *or* THF, RT→70 °C, 17 h, 48% (**15**).

nylamine in THF (Scheme 2). The reactions with phosgene were not clean and required extensive purification. Therefore, we explored additional methods for the formation of compounds **4**, **5**, **9**, **10**, and **14**. Indeed, activation of the pyrazoles as the 2,2,2-trichloroethyl carbamates **34** and **35** and subsequent microwave irradiation in the presence of respective amines in DMF gave the final products **4**, **5**, **9**, **10**, and **14** in 19–86% yield (Scheme 3). Amine **37**, used in the final step of the syntheses of ureas **9** and **10**, was prepared by starting from nicotinoyl chloride hydrochloride and 4-nitroaniline in the presence of pyridine (py). Subsequently, the nitro compound **36** was reduced by catalytic hydrogenation (Pd/C) to yield the desired aniline **37** (Scheme 4).

The pyrazole starting materials **38**–**41** for the preparation of compounds **2**, **3**, **6**, and **16** were conveniently synthesized from the respective hydrazines **42** and **43** and benzoylacetonitriles **44**–**47** in methanol using microwave irradiation (Scheme 5). Pyrazoles **38**–**41** were obtained in 44–71% yields. The pyrazoles were subsequently allowed to react with 4-(benzyloxy)phenyl isocyanate **25** to give ureas **2**, **3**, **6**, and **16** in 48–66% yields. Similarly, urea **17** was synthesized by starting

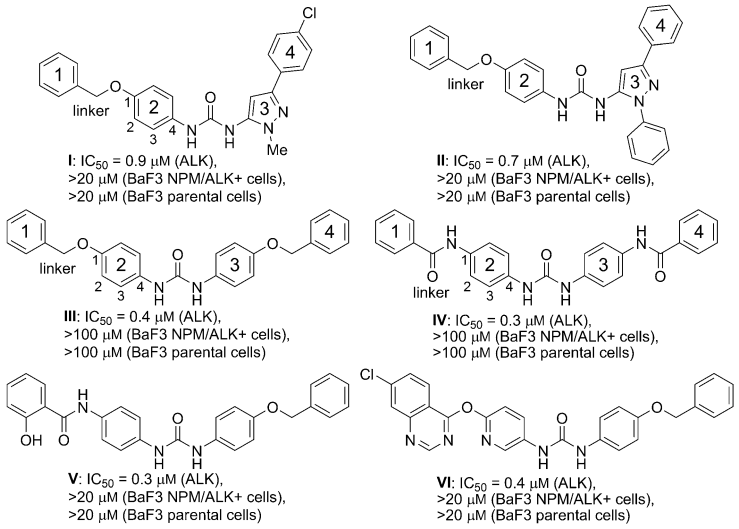

Figure 3. Candidate inhibitors **I**–**VI** from virtual screening. The IC_{50} values derived from inhibition of recombinant ALK and data from cell proliferation inhibition assays are shown.

from pyrazole **48** and isocyanate **25**, with a 40% yield (Table 2, Scheme 5).

Urea formation of the third series of compounds **18**–**20** and **23** and **24** (Table 3) was performed by using isocyanates **25**, **26** and **28** and amines **37** and **49**–**51** (Scheme 6). Synthesis of derivative **21** required aniline **52** to be prepared in two steps from nicotinic acid (Scheme 7). Conventional procedures for amidation (acyl chloride, amine, and 4-(dimethylamino)pyridine (DMAP) or pyridine or triethylamine) gave traces of the desired amide (**53**). The use of other bases such as sodium hydroxide and sodium hydride[30] was also explored, but all the attempted reactions failed to give satisfactory yields of the amide. Therefore, we tried amide coupling reagents, and indeed, 1,1′-carbonyldiimidazole (CDI) worked well, giving **53** in 38% yield. Catalytic hydrogenation (Pd/C) of the nitro compound **53** under reflux gave a modest yield (14%) of the aniline **52**. However, with palladium-catalyzed silicon hydride reduction of the nitro group [poly(methylhydrosiloxane) PMHS, $Pd(OAc)_2$, KF (aq, 1 M) in THF],[31] aniline **52** was obtained in 33% yield. This aniline was subsequently treated with 4-(benzyloxy)phenyl isocyanate **25** to give the urea **21** in 51% yield. Benzamide **54**, for preparation of urea **22**, was synthesized in two steps by starting from aniline and 4-nitrobenzoyl chloride in the presence of DMAP as a nucleophilic catalyst to yield compound **55** (Scheme 8). The nitro amide **55** was catalytically hydrogenated (Pd/C) to the aniline, which was subsequently treated with 4-(benzyloxy)phenyl isocyanate **25** to give the urea product **22** in 85% yield.

Table 1. IC_{50} values of the synthesized pyrazolyl urea derivatives determined in cell-free assays using purified recombinant ALK, and in cell proliferation assays.

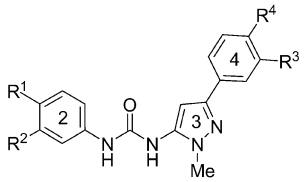

Compd	R^1	R^2	R^3	R^4	IC_{50} [μM][a] ALK	BaF3 Parental	BaF3-NPM–ALK
1	BnO	H	H	H	2.3±0.3	74±4	49±3
2	BnO	H	H	Me	4.3±1.9	>100	>100
3	BnO	H	H	OMe	4.5±1.2	4.1±0.1	4.6±1.1
4	BnO	Cl	H	Cl	2.6±0.2	3.1±1.4	1.8±1.4
5	4-Cl-BnO	H	H	Cl	0.79±0.07	>100	>100
6	BnO	H	Cl	H	0.82±0.03	3.0±0.6	1.4±0.1
7	PhO	H	H	Cl	2.5±0.05	16±7	5±2
8	PhCO	H	H	Cl	4.1±2.1	0.6±0.04	2.6±0.4
9	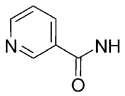	H	H	Cl	15±2	0.14±0.05	0.38±0.04
10	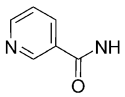	H	H	H	>100	3.5±0.2	7.1±1.1
11	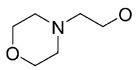	H	H	H	>100	22±7	27±7
12	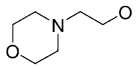	H	H	Cl	41±2	5.0±1.0	3.2±1.3
13	H	Bn	H	Cl	2.3±0.8	25±3	32±2
14[b]	(5-(4-Cl-Ph)-2-Me-2*H*-pyrazol-3-yl)$_2$CO				1.5±0.2	>100	>100

[a] IC_{50} values were determined as described in the Experimental Section and represent the mean ±SEM (n=3). [b] The structure of compound **14** is also shown in Scheme 3 and in the Supporting Information.

Biological activity and structure–activity relationships of synthesized urea compounds

The synthesized compounds had a purity of at least 97% and were submitted to two in vitro tests: an inhibition assay using the isolated enzyme and a proliferation inhibition assay using NPM–ALK-transfected BaF3 cells. Non-transfected BaF3 cell lines were used as a control. The biological data are summarized in Tables 1–3. In a first step, the virtual screening hit **I** (IC_{50}=0.9 μM, no activity on cells) was derivatized (Figure 3 and Table 1).

In compound **1** of this series, the *para*-chloro function of ring 4 was removed to determine the contribution of this

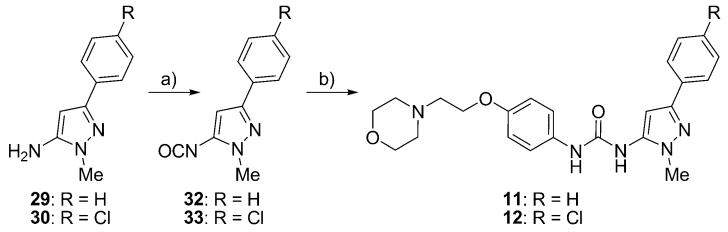

Scheme 2. *Reagents and conditions*: a) $COCl_2$ (20% in PhMe), $NaHCO_3$ (aq, satd)/CH_2Cl_2 (1:1), 0 °C, 15 min; b) 4-(2-morpholin-4-ylethoxy)phenylamine, THF, RT, 24 h, 13–18%.

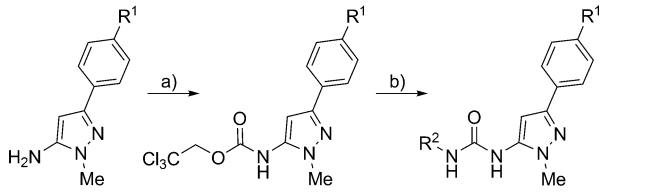

Scheme 3. *Reagents and conditions*: a) Cl_3CCH_2OCOCl, NaOH (aq, 2 M)/EtOAc (1:1), 0 °C→RT, 3.5 h, 71–81%; b) amine, DMF, mw, 100–130 °C, 30–90 min, 19–86%.

halogen to the activity of **I** (Figure 3, Table 1). Removal of the chlorine decreased the inhibitory activity toward the purified enzyme by a factor of ~2–3, indicating that a chlorine substituent at this position of the molecule is favorable. Compound **1** was used to verify the mechanism of action for this series of inhibitors. Double reciprocal plots of compound **1** versus ATP show that these molecules behave as mixed-type inhibitors for ALK (figure S2 in Supporting Information). The activity of compound **2**, in which

Table 2. IC_{50} values of the synthesized pyrazolyl urea derivatives determined in vitro on recombinant ALK and in cell proliferation.

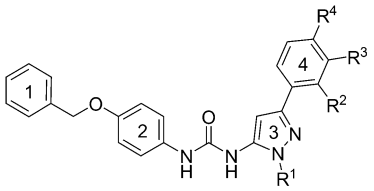

Compd	R^1	R^2	R^3	R^4	IC_{50} [μM][a] ALK	BaF3 Parental	BaF3-NPM–ALK
15	H	H	H	OMe	1.8 ± 0.5	> 100	> 100
16	Ph	H	H	Cl	1.7 ± 0.1	8.4 ± 2.2	1.4 ± 0.4
17	Ph	Cl	H	H	0.61 ± 0.28	5.4 ± 1.5	0.70 ± 0.22

[a] IC_{50} values were determined as described in the Experimental Section and represent the mean ± SEM ($n = 3$).

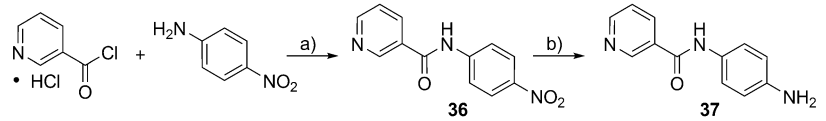

Scheme 4. *Reagents and conditions*: a) py, CH_2Cl_2, 0 °C→RT, 17 h, 33%; b) H_2, Pd/C (10%), EtOH/THF (2:1), RT, 1.5 h, 72%.

the *para*-chlorine of ring 4 of **I** is replaced by a *para*-methyl substituent is even slightly worse than compound **1**, bearing only a hydrogen at this position, indicating that the *para*-chlorine is probably involved in halogen bonding to a water molecule. Furthermore, the lack of cellular activity for this compound suggests that purely hydrophobic substituents at the *para* position of ring 4 are unfavorable for cell penetration. If the methyl group of compound **2** is replaced by a methoxy group (compound **3**), cellular activity is improved by a factor of 18 relative to compound **1**. As compounds **1**–**3** in comparison with **I** have shown that the chlorine of **I** at R^4 is most favorable in terms of enzymatic activity, we decided to modify groups R^1 and R^2 of the scaffold in our endeavor to ameliorate cellular activity. In compound **4** a chlorine was added as the R^2 group which indeed shows good cellular activity, with enzymatic activity similar to that of compound **1**. According to modeling, ring 2 is in close proximity to the gatekeeper residue L256. The slightly lower activity of compound **4** relative to **I** could be explained that in order to accommodate the chlorine, ring 2 needs to tilt slightly, or small conformational changes

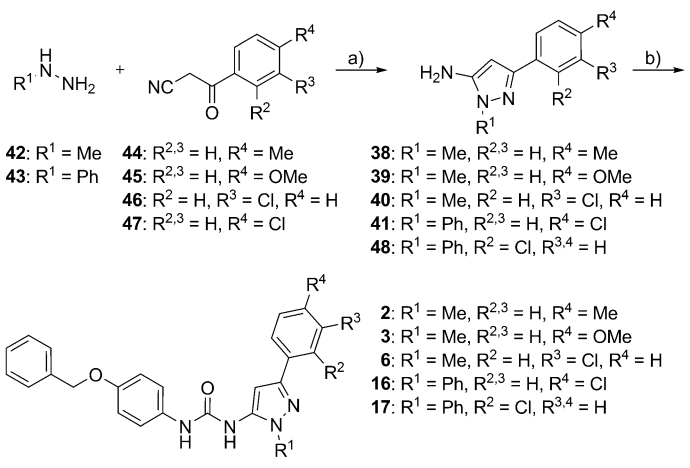

Scheme 5. *Reagents and conditions*: a) MeOH, 120 °C, mw, 40 min, 44–71%; b) 4-BnO-(C_6H_4)NCO (**25**), THF, RT, 15–22 h, 62–66% (**2**, **3**, **6**) *or* 4-BnO(C_6H_4)NCO (**25**), 1,4-dioxane *or* THF, mw, 70 °C, 60–120 min→RT, 16–21 h, 40–48% (**16**, **17**).

Table 3. IC_{50} values of the synthesized phenyl urea derivatives determined using purified ALK kinase domain, and the effects of these compounds on cell proliferation.

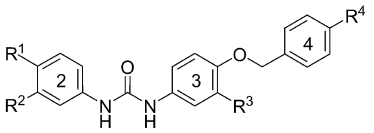

Compd	R^1	R^2	R^3	R^4	IC_{50} [μM][a] ALK	BaF3 Parental	BaF3-NPM–ALK
18	BnO	Cl	H	H	1.7±0.2	44±6	50±8
19	PhO	H	Cl	H	5.0±0.2	10±5	1.5±0.9
20	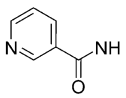	H	H	H	0.80±0.12	61±13	42±5
21	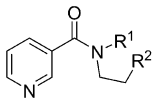		H	H	3.6±0.7	>100	86±1
22	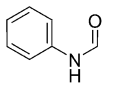	H	H	H	0.39±0.1	>100	>100
23	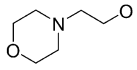	H	H	H	8.9±3.2	>100	>100
24	H	Bn	H	Cl	2.0±0.4	7.1±0.2	11±1

[a] IC_{50} values were determined as described in the Experimental Section and represent the mean ±SEM (n=3).

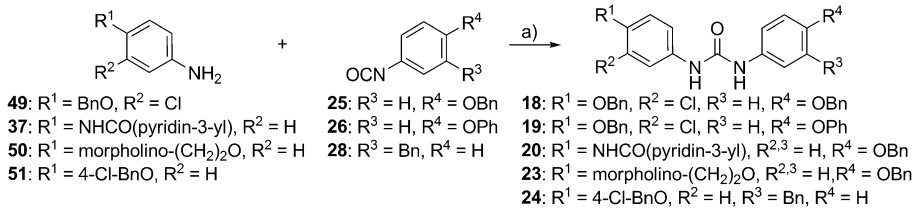

Scheme 6. *Reagents and conditions*: a) CH_2Cl_2 *or* THF, RT, 12–30 h, 41–87%.

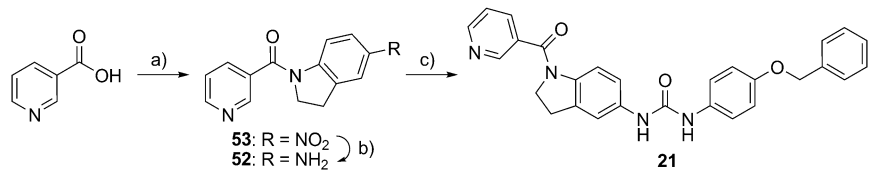

Scheme 7. *Reagents and conditions*: a) 1. CDI, DMF, RT, 1 h, 2. 5-nitroindoline, RT→60 °C, 46 h, 38%; b) 1. $Pd(OAc)_2$, KF (aq, 1 M), THF, 2. PMHS, RT→60 °C, 20 h, 33%; c) 4-BnO(C_6H_4)NCO (**25**), CH_2Cl_2, RT, 18 h, 51%.

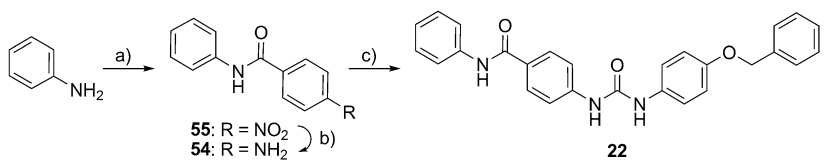

Scheme 8. *Reagents and conditions*: a) 4-nitrobenzoyl chloride, DMAP, THF, RT, 6 h, 71%; b) H_2, Pd/C (10%), MeOH/EtOAc (2:1), RT, 12 h, 59%; c) 4-BnO(C_6H_4)NCO (**25**), THF, RT, 12 h, 85%.

in the protein around the gatekeeper residue are required. When adding a chlorine at the *para* position of ring 1 of **I** (compound **5**) instead of the R^2 position, the potency toward the purified enzyme is slightly improved, but the compound is not active on cells. In contrast, moving the chlorine from the *para* to the *meta* position of ring 4 not only yields favorable activity on the enzyme, but also shows remarkably improved cellular activity (compound **6**).

To investigate whether cellular activity can be improved, the linker and ring 1 of **I** was altered (Figure 3). Shortening the linker by one carbon atom (compound **7**), thereby making it more rigid, slightly decreased potency, but was again beneficial for cell permeability. Furthermore, this compound showed the best ratio obtained thus far between BaF3 parental cells and NPM–ALK-positive cells. For compound **8**, the oxygen linker of compound **7** was replaced by a carbonyl group, making the substituent even more rigid. Whereas activity toward the enzyme slightly worsened again, which is probably due to the fact that it cannot adopt an optimal position in the active site of ALK, compound **8** was very potent toward cells. The four last compounds (**9**–**12**) of this series were synthesized in an attempt to establish an additional hydrogen bond with a backbone atom of the hinge region to improve potency. In this line we extended the linker of **I** by keeping it rigid; an amide bond was therefore introduced (compound **9**). In addition, a pyridine ring was introduced instead of the benzene ring in **I**, as modeling suggested that in this way an additional hydrogen bond with the backbone nitrogen of M256 at the hinge region could be established. Unfortunately this was not the case, as compound **9** showed worse ac-

tivity toward the enzyme, as was the case for compound **8**. This is most likely due to the nitrogen atom of the pyridine ring coming to rest in an unfavorable hydrophobic area in the active site, and due to the rigidity of the linker the substituent cannot accommodate. However, with this compound the cellular activity could be improved more than fourfold. Removing the chlorine atom on ring 4 (compound **10**) was an attempt to create a bit more space for the compound so that it could adapt better to the active site of ALK, but this resulted in both a decrease in enzymatic and cellular activity. The fact that the compound was inactive up to 100 μM, and showed only moderate cellular activity, illustrates the immanent role of the *para*-chlorine at ring 4 which is thought to interact with amino acids F305, I306, I230, and F234, forming a favorable hydrophobic environment (Figure 4). In a further effort to establish a hydrogen bond at the hinge region, compounds **11** and **12** (compound **11** without the *para*-chlorine at ring 4) were synthesized. The linker was made more flexible and was extended by one carbon atom, and the pyridine ring of compound **9** was replaced by a morpholino group, analogous to the interaction between doramapimod and p38 MAP kinase. Similar observations could be made as described for compounds **9** and **10**. Compound **13**, in which the substituent at R^1 was removed and a benzyloxy group at R^2 was introduced instead, shows that similar enzymatic activity could be obtained by either substituting R^1 or R^2. Whether equally favorable cellular activity can be obtained remains to be determined in follow-up compounds of this series currently in preparation. Finally, compound **14**, the last compound of this series, although inactive at the cellular level, shows the symmetric nature of the active site and the resulting challenge to predict the correct binding mode of urea derivatives. In conclusion, with this series of 1-methylpyrazolyl urea derivatives we were able to improve cellular activity from inactive to active at the sub-micromolar level. Furthermore, we show for the first time that urea derivatives are a promising class of compounds to inhibit ALK, for which only few compounds have so far been described as inhibitors. Unfortunately, no additional hydrogen bond interactions with the protein could be established, most probably due to a difference in conformation of the hinge region of ALK relative to that of MAP kinase as a result of the difference in length of this segment between the two proteins. Therefore, further refinements of the model are required for generating a more potent compound from this series in a second round of synthesis, where the lessons learned from the compounds described above will be of great importance.

Compounds **15**–**17** (Table 2) were prepared in order to determine the importance of the methyl group at the pyrazole ring of **I**. In compound **15**, the methyl group at the pyrazole ring was removed relative to compound **3**, leading to a polar NH group at this position. Although this modification was well tolerated regarding enzymatic activity compared with **3** (activity slightly improved from 4.5 to 1.8 μM), the compound is completely inactive on cells. This observation suggests that a polar group at this position is detrimental for cellular activity. Further support for this fact comes from compounds **16** and **17**, in which the methyl group of **I** is substituted by a phenyl ring and where cellular activity is restored. In addition, compound **17**, with a chlorine atom at the *ortho* position of ring 4, shows a remarkable 10-fold selectivity in favor of BaF3 NPM–ALK-positive cells over BaF3 parental cells.

To better characterize the activity of compound **17** in NPM–ALK-positive cells, proliferation and apoptosis assays were carried out using the human ALCL-derived cell line SUDHL-1. As shown in Figure 5A, compound **17** inhibited SUDHL-1 cell growth with an IC_{50} value of 0.8 μM, similar to the case with BaF3-NPM–ALK cells. The compound was less toxic toward NPM–ALK-negative human leukemic cells U937 ($IC_{50} = 3.2$ μM). Compound **17** induced cell death in SUDHL-1 cells, as indicated by annexin V staining (Figure 5B). These effects correlated with a specific block of NPM–ALK autophosphorylation at Y664 (Figure 5C), which is a marker of kinase activation.[32] These data open interesting new perspectives for further improvements in second-round derivatives.

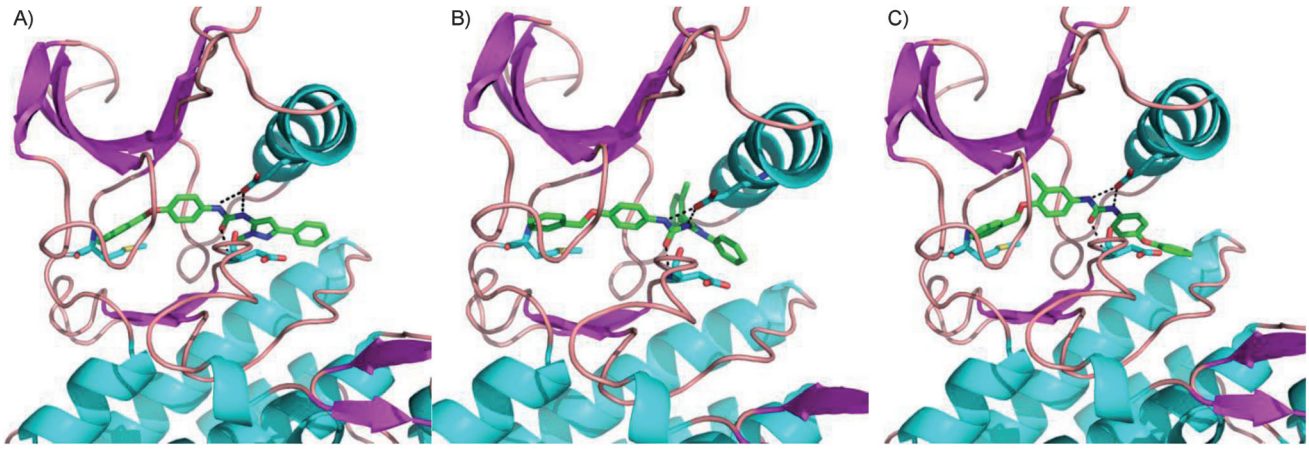

Figure 4. Binding mode of representative urea derivatives as depicted by docking into the inactive ALK model. M259 of the hinge region, E227 of α-helix C and D330 of the DFG motif are shown as sticks with carbon atoms in cyan. Hydrogen bonds are shown as black dotted lines. For the sake of clarity, the gatekeeper L256 is not displayed. A) Compound **1** representing the 1-methylpyrazolyl urea derivatives. B) Compound **17** representing the 1-phenylpyrazolyl urea derivatives. C) Compound **19** representing the phenyl urea derivatives.

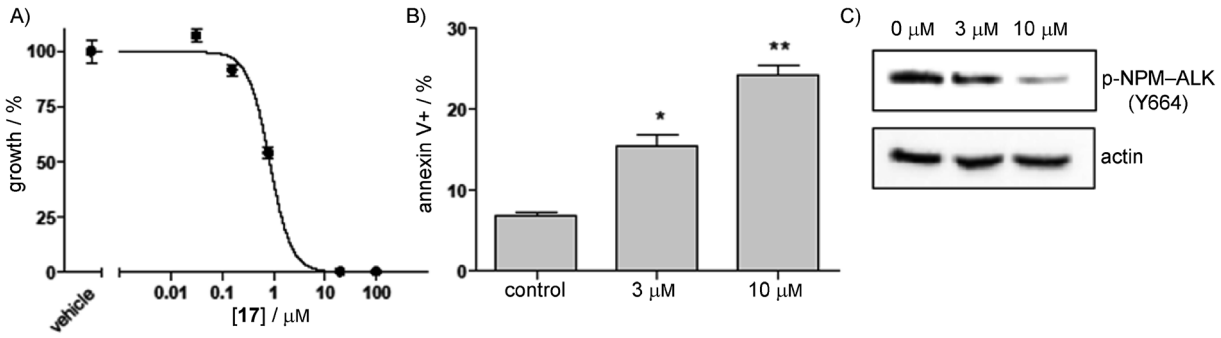

Figure 5. Activity of compound **17** in SUDHL-1 cells. A) Inhibition of cellular growth was determined with increasing doses of inhibitor **17** by [^{3}H]thymidine incorporation assay and values are reported as a percentage of vehicle-treated control. B) SUDHL-1 cells were treated with vehicle or **17** at the indicated concentrations for 24 h; apoptosis is shown as a percent of annexin V-positive cells in the cell culture. C) NPM–ALK autophosphorylation was monitored by anti-pY664 antibody; equal gel loading is verified by actin staining; $*p < 0.05$ versus control; $**p < 0.01$ versus control.

To explore the potential of the central 1,3-diphenylurea scaffold of the screening hits **III**–**V**, a series of derivatives was prepared (Table 3). Compound **18**, a derivative of **III** with an additional chlorine at position R^2, which, according to the modeling, is expected to make favorable nonpolar interactions with the gatekeeper residue, exhibits only low activity in cell-based assays, but is rather potent on the enzymatic level. Compound **19**, with a phenoxy substituent at R^1 and a chlorine at ring 3, is selective against NPM–ALK-positive cells (greater than sevenfold), indicating that the position of the chlorine offers an additional possibility for the synthesis of new selective compounds. It has the best cellular activity obtained for this series. Compounds **20**–**23** were synthesized in an attempt to establish an additional hydrogen bond with the hinge region (similar to compounds **9**–**12**, which were not successful for the same reasons already indicated for the 1-methylpyrazolyl urea derivatives). In addition, compounds **20**–**23** are only moderately active or inactive toward cells. Finally, for compound **24** a similar approach was used as with compound **16** to exemplify that nonpolar substituents at either R^1 or R^2 lead to similar enzymatic activities. The scaffold explored in Table 3 seems to be less favorable in terms of cell permeability, but considering the small number of derivatives, more compounds probably need to be synthesized in order to draw a final conclusion. No significant improvement of the enzymatic activity relative to the underlying screening hits was observed. The positive feature about the core scaffold of compounds listed in Table 3 is that it is more permissive than those shown in Tables 1 and 2. However, its symmetric nature makes binding mode elucidations more difficult.

Conclusions

A series of new inhibitors targeted to the catalytic site of ALK were designed, synthesized, and screened for biological activity. These novel ALK inhibitors have IC_{50} values as low as 390 nM. More importantly, three derivatives (compounds **16**, **17**, and **19**) preferentially inhibited the growth of NPM–ALK-transfected cells. These results support the development of urea-based compounds as potent, selective, and cell-permeable ALK inhibitors.

Experimental Section

Materials and general procedures

All reagents were commercially available and were acquired from ABCR (Karlsruhe, Germany), Asdi (Newark, NJ, USA), BDH (Poole, UK), Fluka (Buchs, Switzerland), Matrix Scientific (Columbia, SC, USA), Maybridge (Cambridge, UK) and Sigma–Aldrich (Schnelldorf, Germany). THF and Et_2O were distilled from sodium/benzophenone ketyl. $CHCl_3$ was distilled from CaH_2. Anhydrous DMF was from Fluka (Buchs, Switzerland) and was stored over molecular sieves (4 Å) under an inert atmosphere of dry argon. All reactions in anhydrous solvents were performed in flame-dried glassware under an inert atmosphere of dry argon. The progress of chemical reactions was monitored by thin-layer chromatography (TLC) on silica gel 60 F_{254} plates (Merck; Darmstadt, Germany) using phosphomolybdic acid stain (10% by weight in EtOH) or ninhydrin stain (1.5% by weight in EtOH). Flash SiO_2 column chromatography was performed with Merck silica gel 60 (230–400 mesh) or with a Biotage high-performance flash chromatography Sp^4 system (Uppsala, Sweden) using a 0.1 mm pathlength flow cell UV detector/recorder module (fixed wavelength: 254 nm), 12 mm or 25 mm flash cartridges, and the indicated mobile phase.

^{1}H NMR, ^{13}C NMR, and DEPT spectra were recorded on a Varian Mercury 300 MHz or a Varian Unity 500 MHz spectrometer (Varian, Palo Alto, CA, USA) as solutions in $CDCl_3$, [D_6]DMSO, or CD_3OD. Deuterated solvents were purchased from Sigma. Chemical shifts (δ) are given ppm relative to the NMR solvent signals ($CDCl_3$: 7.26 and 77.21 ppm, [D_6]DMSO: 2.50 and 39.52 ppm, CD_3OD: 3.31 and 49.00 ppm for ^{1}H and ^{13}C NMR, respectively). Multiplicities are indicated by br s (broad singlet), s (singlet), d (doublet), dt (doublet of triplets), ddd (doublet of doublet of doublet), m (multiplet), and t (triplet).

HPLC–MS analysis of the synthesized compounds was performed to determine the purity of each compound using methods A, B, or C. For method A, an Agilent 1100 series HPLC instrument (Agilent Technologies, Palo Alto, CA) with a UV detector (λ 210 nm) and an Esquire-LC quadrupole ion trap mass spectrometer equipped with an ESI interface (Bruker Daltonics, Bremen, Germany) and LC–MSD Trap software, version 5.2 (Bruker Daltonics) was used. Signal separation was performed using a Phenomenex Luna C8(2) column (2.0×150 mm, 5.0 μm). The column was operated at a constant temperature of 40 °C. The eluent consisted of H_2O (plus 0.1% formic acid, solvent A) and 2-propanol (plus 0.1% formic acid, solvent B) and a gradient run was performed (95:5→0:100 over

35 min and 0:100 for 10 min). For method B, an Agilent 1100 series HPLC instrument (Agilent Technologies) with a UV detector (λ 210 nm) and a PerkinElmer Sciex API3000 triple-quadrupole LC–MS–MS mass spectrometer (Applied Biosystems/MDS Sciex, Concord, ON, Canada) with a turbo ESI source was used. Signal separation was carried out by an XTerra MS RP18 column (4.6×30 mm, 2.5 μm). The column was operated at a constant temperature of 35 °C. The eluent consisted of H_2O (plus 0.1% formic acid, solvent A) and 2-propanol (plus 0.1% formic acid, solvent B) and a gradient run was performed (95:5 for 1 min, 95:5→0:100 over 24 min, and 0:100 for 4 min). Method C was otherwise the same as method B except that the column temperature was kept at 40 °C, and the eluent consisted of H_2O (plus 0.1% formic acid, solvent A) and acetonitrile (solvent B). An isocratic run was performed (95:5 for 40 min).

Fourier transform infrared (FTIR) spectra were recorded using a Vertex 70 spectrometer (Bruker Optik GmbH, Ettlingen, Germany) and MIRacle™ ATR accessory (Pike Technologies, Madison, WI, USA) or from a KBr tablet. Melting points were measured with an Electrothermal IA 9100 apparatus and are uncorrected. Purity of all tested compounds was >97%.

Molecular modeling

Homology model: A model of ALK corresponding to a closed (inactive) conformation of the catalytic site was generated using the following protocol. The sequences of human ALK were retrieved from the SwissProt database[33] (accession code Q9M73). The tyrosine kinase sequence of human ALK, spanning 278 residues, was taken as a query to search the RCSB Protein Data Bank (PDB) using PSI-Blast[34] to find putative templates for ALK homology modeling. Further filtering criteria were applied, including preferences for high-resolution X-ray structures, gapless backbones, and high sequence identity/similarity. Finally, the following templates were chosen to generate model of ALK: mouse c-Abl (PDB IDs: 1IEP, 1OPJ) and human insulin receptor (INSR) mutant (PDB ID: 1IRK). ALK shares 34% identity and 48% similarity with Abl, and 40% identity and 56% similarity with INSR. Reliable pairwise sequence–structure alignments, which were necessary for accurate homology modeling, were obtained using the Verta algorithm of the Superimposer plug-in in the program Bodil.[35] These pairwise alignments were merged to multiple alignments in the program *malign*[36] using the STRMAT110 substitution matrix.[37] Homology modeling was performed with the program Modeller6v2[38] using default parameters, including a round of minimization. For each conformation, 100 models were generated, and their overall geometrical quality was assessed by Procheck.[39] The models showing geometrical qualities similar to the templates were chosen for docking studies. For binding mode evaluation of urea derivatives, models of the active and inactive conformation of ALK were used. Docking of the urea compounds into the active model did not result in any plausible binding orientations that could support the experimental data.

Molecular docking: All dockings were performed using the programs Gold[40] and FlexX.[41] The active site of the ALK model was defined by superimposing it onto the crystal structure of PDB ID: 1IEP and taking into account all residues of the ALK model corresponding to the amino acids of Abl positioned 6.5 Å around imatinib of 1IEP. Thirty docking solutions were generated per docking run with FlexX and ten per docking run with Gold. A general consensus in the docking poses has been observed between FlexX and Gold.

Virtual screening: The virtual screen was performed on a subset of the ZINC database consisting of ~40000 compounds of a Maybridge (part of Thermo Fisher Scientific™) lead-like compound library complying with Lipinski's rule of five. Initial binding poses in the inactive model of ALK were obtained using the program Dock (v. 4.0), which is particularly suited to dock large compound databases with a good balance between accuracy and speed. The active site of ALK for the virtual screening was defined as outlined above in the *Molecular docking* section, and no further constraints were applied. The obtained binding poses were subjected to consensus scoring as implemented in Sybyl 6.3 (Tripos). After visual inspection (to exclude binding poses that do not occupy most parts of the active site) the best 1000 poses were chosen for a second docking round using FlexX. The resulting poses were again consensus scored, and the 20 top-ranked compounds were ordered and tested experimentally for inhibitory activity against ALK. The urea derivatives among these hits were finally used as starting points for the synthesis of new derivatives described in the current study.

Synthesis of compounds

One representative synthesis of each procedure used to prepare the intermediates and products is presented here (urea derivatives **1**, **9**, **12**, **16**, **17**, **20**–**22**, and intermediates **35**–**37**, **41**, and **52**–**55**). Procedures for the synthesis and analysis of the remaining compounds are available in the Supporting Information.

1-[4-(Benzyloxy)phenyl]-3-(1-methyl-3-phenyl-1*H*-pyrazol-5-yl)urea (1): A solution of 4-(benzyloxy)phenyl isocyanate (0.25 g, 1.1 mmol, 1.1 equiv) and 5-amino-1-methyl-3-phenylpyrazole (0.17 g, 1.0 mmol) in THF (10 mL) was stirred at RT for 12 h. The solvent was evaporated in vacuo, and the solid residue was washed with a mixture of cold *n*-hexane and THF (1:1, 2×5 mL) and filtered. The crude product was recrystallized from a mixture of *n*-hexane and THF (2:1) to give a white solid (compound **1**; 0.36 g, 90% yield). ^{1}H NMR (300 MHz, [D$_6$]DMSO): δ=8.74 (s, 1H), 8.58 (s, 1H), 7.79–7.71 (m, 2H), 7.48–7.22 (m, 10H), 7.00–6.91 (m, 2H), 6.61 (s, 1H), 5.07 (s, 2H), 3.72 ppm (s, 3H); ^{13}C NMR (75 MHz, [D$_6$]DMSO): δ=153.7, 151.9, 148.0, 138.6, 137.6, 133.6, 132.6, 128.6, 128.4, 127.7, 127.6, 127.3, 124.7, 120.1, 115.0, 94.6, 69.4, 35.4 ppm; LC–MS: (398.17) *m/z* 399.2 $[M+H]^+$, 412.2 $[M+Na]^+$; t_R=28.1 min, purity 99% (method A).

***N*-[4-[3-[3-(4-Chlorophenyl)-1-methyl-1*H*-pyrazol-5-yl]ureido]phenyl]nicotinamide (9):** A solution of compounds **35** (0.13 g, 0.33 mmol) and **37** (0.10 g, 0.47 mmol, 1.3 equiv) in DMF (3 mL) was irradiated under mw at 100 °C for 30 min. H_2O (20 mL) was added to the reaction mixture, and the precipitate was filtered. The solid was collected and purified by flash SiO_2 column chromatography ($CHCl_3$/MeOH, 1:0→10:1) to give a pink solid (compound **9**; 0.05 g, 32% yield); mp: 233 °C (dec); ^{1}H NMR (300 MHz, [D$_6$]DMSO): δ=10.34 (s, 1H), 9.07 (s, 1H), 8.90 (s, 1H), 8.72 (d, 1H, J=4.7 Hz), 8.66 (s, 1H), 8.25 (d, 1H, J=7.7 Hz), 7.74 (d, 2H, J=8.3 Hz), 7.66 (d, 2H, J=8.4 Hz), 7.53 (dd, 1H, J=7.6, 5.1 Hz), 7.48–7.37 (m, 4H), 6.63 (s, 1H), 3.70 ppm (s, 3H); ^{13}C NMR (75 MHz, [D$_6$]DMSO): δ=163.7, 152.0, 151.8, 148.6, 146.9, 138.8, 135.5, 135.4, 133.4, 132.5, 131.7, 130.6, 128.6, 126.4, 123.4, 121.1, 118.6, 94.7, 35.5 ppm; IR (KBr): $\tilde{\nu}$=3288, 3151, 3054, 1686, 1646, 1565 cm^{-1}; LC–MS (446.13): *m/z* 447.1 $[M+H]^+$, t_R=14.4 min, purity >99% (method B).

1-[3-(4-Chlorophenyl)-1-methyl-1*H*-pyrazol-5-yl]-3-[4-(2-morpholinoethoxy)phenyl]urea (12): A mixture of 3-(4-chlorophenyl)-1-methyl-1*H*-pyrazol-5-ylamine (0.21 g, 1.0 mmol), CH_2Cl_2 (14 mL) and a saturated solution of $NaHCO_3$ (14 mL) was cooled to 0 °C. Phos-

gene (2.0 mL, 20% in toluene, 4 equiv) was added, and the reaction mixture was stirred at 0 °C for 15 min. The CH_2Cl_2 phase was separated, dried (Na_2SO_4) and evaporated in vacuo. CH_2Cl_2 (5 mL) and 4-(2-morpholino-4-ylethoxy)phenylamine (0.20 g, 0.89 mmol, 0.89 equiv) was added to the solid, and the resulting reaction mixture was stirred at RT for 24 h. The reaction mixture was filtered, and the crude product was purified by flash SiO_2 column chromatography (Biotage MPLC, $CHCl_3$/MeOH, 4:1) to give a white solid (compound **12**; 0.08 g, 18% yield). ^{1}H NMR (300 MHz, [D$_6$]DMSO): δ = 8.75 (s, 1H), 8.63 (s, 1H), 7.77 (d, 1H, J = 8.4 Hz), 7.43 (d, 2H, J = 8.3 Hz), 7.36 (d, 2H, J = 8.9 Hz), 6.88 (d, 2H, J = 8.9 Hz), 6.63 (s, 1H), 4.04 (t, 2H, J = 5.8 Hz), 3.72 (s, 3H), 3.57 (t, 4H, J = 4.6 Hz), 2.66 (t, 2H, J = 5.7 Hz), 2.46 ppm (t, 4H, J = 4.6 Hz); ^{13}C NMR (75 MHz, [D$_6$]DMSO): δ = 153.8, 151.9, 146.9, 138.9, 132.5, 132.4, 131.7, 128.6, 126.4, 120.1, 114.7, 94.7, 66.2, 65.5, 57.1, 53.6, 35.5 ppm; LC–MS (455.17): m/z 456.2 $[M+H]^+$, 478.2 $[M+Na]^+$; t_R = 18.9 min, purity > 99% (method A).

1-[4-(Benzyloxy)phenyl]-3-[3-(4-chlorophenyl)-1-phenyl-1*H*-pyrazol-5-yl]urea (16): A solution of compound **41** (0.083 g, 0.31 mmol) and 4-(benzyloxy)phenyl isocyanate (0.069 g, 0.31 mmol) in 1,4-dioxane (3 mL) was irradiated under mw at 70 °C for 120 min and stirred at RT for 16 h. The reaction mixture was evaporated in vacuo, and the crude product was purified by flash SiO_2 column chromatography (Biotage MPLC, *n*-hexane/EtOAc, 4:1→1:1) to give a white solid (compound **16**; 0.073 g, 48% yield). ^{1}H NMR (300 MHz, [D$_6$]DMSO); ^{1}H NMR (300 MHz, [D$_6$]DMSO): δ = 8.88 (br s, 1H), 8.49 (br s, 1H), 7.87 (d, 2H, J = 8.7 Hz), 7.77 (d, 2H, J = 8.7 Hz), 7.68–7.27 (m, 12H), 6.97–6.88 (m, 3H), 5.05 ppm (s, 2H); ^{13}C NMR (75 MHz, [D$_6$]DMSO): δ = 153.7, 151.7, 149.0, 138.9, 137.3, 132.5, 132.3, 132.0, 129.4, 128.7, 128.4, 128.0, 127.7, 127.6, 126.8, 124.7, 120.0, 115.0, 96.1, 69.4 ppm; LC–MS (494.15): m/z 495.1 $[M+H]^+$, t_R = 19.4 min, purity 98% (method B).

1-[4-(Benzyloxy)phenyl]-3-[3-(2-chlorophenyl)-1-phenyl-1*H*-pyrazol-5-yl]urea (17): Following the procedure for compound **16**, urea derivative **17** was synthesized from a solution of 3-(2-chlorophenyl)-1-phenyl-1*H*-pyrazol-5-ylamine (0.10 g, 0.37 mmol) and 4-(benzyloxy)phenyl isocyanate (0.084 g, 0.37 mmol) in THF (4 mL), which was irradiated under mw at 70 °C for 60 min and stirred at RT for 21 h. The crude product was recrystallized from THF and washed with *n*-hexane to give a white solid (compound **17**; 0.074 g, 40% yield). ^{1}H NMR (300 MHz, [D$_6$]DMSO): δ = 8.91 (br s, 1H), 8.52 (br s, 1H), 7.88–7.84 (m, 1H), 7.67–7.29 (m, 15H), 6.98 (s, 1H), 6.93 (d, 2H, J = 9.0 Hz), 5.05 ppm (s, 2H); ^{13}C NMR (75 MHz, [D$_6$]DMSO): δ = 153.7, 151.6, 147.9, 138.1, 138.0, 137.2, 132.5, 131.8, 131.1, 130.3, 129.4, 128.4, 128.0, 127.7, 127.6, 127.3, 124.6, 120.0, 115.0, 99.3, 69.4 ppm; LC–MS (494.15): m/z 495.1 $[M+H]^+$; t_R = 18.8 min, purity 98% (method B).

***N*-[4-[3-[4-(Benzyloxy)phenyl]ureido]phenyl]nicotinamide (20):** Urea derivative **20** was synthesized from a solution of **37** (0.10 g, 0.49 mmol, 1.1 equiv) and 4-(benzyloxy)phenyl isocyanate (0.10 g, 0.44 mmol) in THF (11 mL), which was stirred at RT for 18 h. The reaction mixture was filtered, and the crude product was purified by flash SiO_2 column chromatography (Biotage MPLC, $CHCl_3$/MeOH, 1:0→10:1) to give a white solid (compound **20**; 0.080 g, 41% yield). ^{1}H NMR (300 MHz, [D$_6$]DMSO): δ = 10.34 (s, 1H), 9.10 (dd, 1H, J = 2.2, 0.7 Hz), 8.75 (dd, 1H, J = 4.8, 1.6 Hz), 8.59 (br s, 1H), 8.48 (br s, 1H), 8.28 (dt, 1H, J = 8.0, 2.2 Hz), 7.66 (d, 2H, J = 9.0 Hz), 7.56 (ddd, 1H, J = 8.0, 4.9, 0.8 Hz), 7.47–7.29 (m, 9H), 6.94 (d, 2H, J = 9.1 Hz), 5.06 ppm (s, 2H); ^{13}C NMR (75 MHz, [D$_6$]DMSO): δ = 163.6, 153.4, 152.7, 152.0, 148.6, 137.3, 136.1, 135.3, 133.0, 132.9, 130.6, 128.4, 127.7, 127.6, 123.5, 121.1, 119.9, 118.3, 115.0, 69.4 ppm; LC–MS (438.17): m/z 439.2 $[M+H]^+$, 461.1 $[M+Na]^+$, t_R = 24.2 min, purity > 99%. (method A).

1-[4-(Benzyloxy)phenyl]-3-(1-nicotinoylindolin-5-yl)urea (21): A solution of 4-(benzyloxy)phenyl isocyanate (0.059 g, 0.26 mmol) and compound **52** (0.063 g, 0.26 mmol) in CH_2Cl_2 (6 mL) was stirred at RT for 18 h. The reaction mixture was filtered, and the solid was washed with a small amount of CH_2Cl_2. The crude product was purified by flash SiO_2 column chromatography (Biotage MPLC, $CHCl_3$/MeOH, 1:0→10:1) to give a pale-yellow solid (compound **21**; 0.062 g, 51% yield), ^{1}H NMR (300 MHz, [D$_6$]DMSO): δ = 8.79 (s, 1H), 8.70 (dd, 1H, J = 4.7, 1.4 Hz), 8.59 (s, 1H), 8.45 (s, 1H), 8.02 (s, 2H), 7.58–7.27 (m, 9H), 7.19 (s, 1H), 7.00–6.86 (m, 2H), 5.06 (s, 2H), 4.02 (t, 2H, J = 7.8 Hz), 3.08 ppm (t, 2H, J = 8.2 Hz); ^{13}C NMR (75 MHz, [D$_6$]DMSO): δ = 165.2, 153.4, 152.7, 150.7, 147.7, 137.3, 136.9, 136.4, 134.7, 133.3, 133.0, 128.4, 127.7, 127.6, 123.5, 119.9, 117.0, 116.5, 115.0, 69.4, 50.5, 28.1 ppm; LC–MS (464.18): m/z 465.2 $[M+H]^+$; t_R = 15.2 min, purity > 99% (method B).

4-[3-[4-(Benzyloxy)phenyl]ureido]-*N*-phenylbenzamide (22): A solution of 4-(benzyloxy)phenyl isocyanate (0.25 g, 1.1 mmol, 1.1 equiv) and compound **54** (0.21 g, 1.0 mmol) in THF (10 mL) was stirred at RT for 12 h. The solvent was evaporated in vacuo, and the solid residue was washed with a mixture of cold *n*-hexane and THF (1:1, 2×5 mL) and filtered. The crude product was recrystallized from a mixture of *n*-hexane and THF (2:1) to give a white solid (compound **22**; 0.37 g, 85% yield). ^{1}H NMR (300 MHz, [D$_6$]DMSO): δ = 10.1 (br s, 1H), 8.95 (br s, 1H), 8.61(br s, 1H), 7.94–6.92 (m, 18H), 5.1 ppm (s, 2H); ^{13}C NMR (75 MHz, [D$_6$]DMSO): δ = 165.0, 153.7, 152.5, 143.1, 139.4, 137.3, 132.6, 128.7, 128.5, 128.4, 127.7, 127.6, 123.3, 120.3, 120.2, 119.8, 117.0, 116.7, 115.0, 69.4 ppm; LC–MS (437.17) m/z 438.3 $[M+H]^+$, 460.2 $[M+Na]^+$; t_R = 27.7 min, purity 97% (method A).

[5-(4-Chlorophenyl)-2-methyl-2*H*-pyrazol-3-yl]carbamic acid 2,2,2-trichloroethyl ester (35): A 2 M solution of NaOH in H_2O (8.0 mL, 16 mmol, 7.5 equiv) was added to a solution of 3-(4-chlorophenyl)-1-methyl-1*H*-pyrazol-5-ylamine (0.48 g, 2.1 mmol) in EtOAc (8 mL) at 0 °C, and the resulting mixture was stirred at 0 °C for 30 min. 2,2,2-Trichloroethyl chloroformate (0.54 mL, 3.8 mmol, 1.8 equiv) was added portionwise at 0 °C over a period of 1 h to this mixture, and the resulting mixture was stirred at RT for 2 h. The aqueous layer was extracted with EtOAc (2×20 mL). The combined organic layers were washed with brine (2×20 mL), dried (Na_2SO_4), filtered and evaporated in vacuo. The crude product was purified by flash SiO_2 column chromatography (*n*-hexane/EtOAc, 1:0→2:1) to give a white solid (compound **35**; 0.66 g, 81% yield); mp: 136 °C; ^{1}H NMR (300 MHz, $CDCl_3$): δ = 7.67 (2H, d, J = 8.4 Hz), 7.34 (2H, d, J = 6.9 Hz), 6.86 (1H, s), 6.49 (1H, s), 4.85 (2H, s), 3.81 ppm (3H, s); ^{13}C NMR (75 MHz, $CDCl_3$): δ = 149.2, 135.5, 133.8, 131.8, 129.0, 126.8, 97.8, 95.0, 75.3, 35.9, 29.9 ppm; IR (KBr): $\tilde{\nu}$ = 3293, 3214, 2955, 1749, 1714 cm^{-1}.

***N*-(4-Nitrophenyl)nicotinamide (36):** A mixture of nicotinoyl chloride hydrochloride (1.9 g, 11 mmol, 1.5 equiv), pyridine (1.3 mL, 16 mmol, 2.3 equiv) and CH_2Cl_2 (20 mL) was stirred at 0 °C for 30 min. 4-Nitroaniline (1.0 g, 7.2 mmol) was added to the mixture, which was slowly warmed to RT and then stirred at RT for 16 h. The solvents were removed, and the crude product was successively washed with warm H_2O and recrystallized from MeOH to give a yellow solid (compound **36**; 0.59 g, 33% yield). ^{1}H NMR (300 MHz, [D$_6$]DMSO): δ = 11.09 (s, 1H), 9.19 (s, 1H), 8.91–8.80 (m, 1H), 8.43 (d, J = 8.0 Hz, 1H), 8.29 (d, J = 9.2 Hz, 2H), 8.07 (d, J = 9.3 Hz, 2H), 7.68 ppm (dd, J = 7.9, 5.0 Hz, 1H); ^{13}C NMR (75 MHz, [D$_6$]DMSO):

δ = 164.5, 151.6, 148.0, 145.0, 142.7, 136.9, 130.4, 124.9, 124.0, 120.0 ppm.

***N*-(4-Aminophenyl)nicotinamide (37):** A mixture of compound **36** (0.21 g, 0.86 mmol) and Pd/C (10%, 0.020 g) in EtOH (40 mL) and THF (20 mL) was hydrogenated at RT for 1.5 h. The reaction mixture was filtered through a pad of Celite 545 and washed with EtOH. The filtrate was evaporated in vacuo, and the crude product was purified by flash SiO_2 column chromatography (Biotage MPLC, $CHCl_3$/MeOH, 1:0→10:1) to give a brown solid (compound **37**; 0.13 g, 72% yield). ^{1}H NMR (300 MHz, [D$_6$]DMSO): δ = 10.06 (s, 1H), 9.06 (s, 1H), 8.72 (d, 1H, J = 4.8 Hz), 8.25 (d, 1H, J = 7.9 Hz), 7.53 (dd, 1H, J = 8.0, 4.8 Hz), 7.37 (d, 2H, J = 8.3 Hz), 6.55 (d, 2H, J = 8.3 Hz), 4.96 ppm (s, 2H); ^{13}C NMR (75 MHz, [D$_6$]DMSO): δ = 163.1, 151.7, 148.5, 145.5, 135.2, 130.9, 127.7, 123.4, 122.2, 113.7 ppm; LC–MS (213.09): *m/z* 214.2 $[M+H]^+$, t_R = 1.6 min, purity >99% (method C).

3-(4-Chlorophenyl)-1-phenyl-1*H*-pyrazol-5-ylamine (41): A mixture of phenylhydrazine hydrochloride (0.250 g, 1.73 mmol) and 4-chlorobenzoylacetonitrile (0.318 g, 1.78 mmol, 1.03 equiv) in MeOH (3 mL) was irradiated under mw at 120 °C for 40 min. The reaction mixture was cooled to RT, and the solvent was evaporated in vacuo. A 2 M solution of NaOH in H_2O (20 mL) was added to the crude product, and the resulting mixture was extracted with CH_2Cl_2 (2×20 mL). The combined organic phases were washed with brine (2×20 mL) and evaporated in vacuo. The crude product was recrystallized from a mixture of *n*-hexane and THF (1:1) to give a white solid (compound **41**; 0.21 g, 44% yield). ^{1}H NMR (300 MHz, $CDCl_3$): δ = 7.75 (d, 2H, J = 8.4 Hz), 7.63 (d, 2H, J = 8.4 Hz), 7.55–7.48 (m, 2H, J = 7.7 Hz), 7.40–7.34 (m, 3H), 5.94 (s, 1H), 3.86 ppm (br s, 2H); ^{13}C NMR (75 MHz, $CDCl_3$): δ = 150.5, 146.1, 138.6, 133.7, 132.1, 129.8, 128.9, 127.9, 127.1, 124.4, 88.2 ppm.

(5-Amino-2,3-dihydroindol-1-yl)pyridin-3-ylmethanone (52): A mixture of compound **53** (0.20 g, 0.74 mmol) and palladium(II) acetate (0.0080 g, 0.037 mmol, 0.05 equiv) in THF (5 mL) was stirred at RT for 10 min. A 1 M solution of KF in H_2O (1.5 mL, 2.0 equiv) was added to the mixture and the resulting mixture was stirred at RT for 5 min. Poly(methylhydrosiloxane) (PMHS) (0.18 mL, 2.0 mmol, 4.0 equiv) was added dropwise at RT over 3 min, and the resulting black solution was stirred at RT for 20 h. PMHS (0.060 mL, 0.67 mmol, 1.3 equiv) was then added dropwise. The reaction mixture was heated at 60 °C for 20 min, and a 1 M solution of KF in H_2O (0.50 mL, 0.66 equiv) was added. Et_2O (20 mL) was added to the mixture and stirred for 5 min. The aqueous layer was then extracted with Et_2O (2×10 mL), the combined organic phases were filtered through Celite 545, and the cake was washed with EtOAc (40 mL). The filtrate was washed with brine (2×30 mL), dried (Na_2SO_4), filtered and evaporated in vacuo. The crude product was purified by SiO_2 flash column chromatography (EtOAc/MeOH, 1:0→0:1) to give a brown solid (compound **52**; 0.058 g, 33% yield). ^{1}H NMR (300 MHz, [D$_6$]DMSO): δ = 8.76 (1H, s), 8.65 (1H, d, J = 3.3 Hz), 7.99 (1H, d, J = 8.1 Hz), 7.81 (1H, d, J = 8.7 Hz), 7.49 (1H, ddd, J = 7.8, 4.9, 0.9 Hz), 6.49 (1H, d, J = 2.1 Hz), 6.42 (1H, d, J = 8.4 Hz), 4.98 (2H, br s), 3.93 (2H, t, J = 1.8 Hz), 2.95 ppm (2H, 1.8 Hz); ^{13}C NMR (75 MHz, [D$_6$]DMSO): δ = 164.2, 150.4, 147.7, 145.9, 134.6, 134.5, 132.5, 123.4, 117.6, 111.7, 110.3, 50.3, 28.1 ppm.

(5-Nitro-2,3-dihydroindol-1-yl)pyridin-3-ylmethanone (53): A solution of nicotinic acid (1.0 g, 8.1 mmol) and 1,1′-carbonyldiimidazole (1.4 g, 8.0 mmol, 0.99 equiv) in DMF (5 mL) was stirred at RT for 1 h. 5-Nitroindoline (1.2 g, 7.1 mmol, 0.87 equiv) was added to the solution and, after 15 min of mixing, the solution was heated at 60 °C for 21 h. DMF (15 mL) and CDI (0.73 g, 4.0 mmol, 0.50 equiv) were added to the reaction mixture. After stirring at 60 °C for 24 h, the reaction mixture was quenched with ice H_2O (30 mL). The resulting mixture was extracted with EtOAc (3× 60 mL), washed with a saturated $NaHCO_3$ solution (2×25 mL), H_2O (2×50 mL) and brine (2×50 mL), dried (Na_2SO_4), filtered and evaporated in vacuo. The crude product was purified by SiO_2 flash column chromatography ($CHCl_3$/MeOH, 10:1→4:1) to give a yellow solid (compound **53**; 0.72 g, 38% yield); mp: 221 °C; ^{1}H NMR (300 MHz, [D$_6$]DMSO): δ = 8.85 (dd, 1H, J = 2.2, 0.8 Hz), 8.74 (dd, 1H, J = 4.9, 1.7 Hz), 8.22–8.16 (m, 2H), 8.11–8.07 (m, 2H, J = 7.9, 2.1, 1.8 Hz), 7.56 (ddd, 1H, J = 7.9, 4.9, 0.9 Hz), 4.15 (t, 2H, J = 8.5 Hz), 3.21 ppm (t, 2H, J = 8.3 Hz); ^{13}C NMR (75 MHz, [D$_6$]DMSO): δ = 167.0, 151.3, 148.3, 147.8, 143.2, 134.8, 132.1, 124.1, 123.5, 120.6, 116.0, 51.2, 27.2 ppm; IR (KBr): $\tilde{\nu}$ = 3262, 3060, 2940, 1642, 1564 cm^{-1}.

4-Amino-*N*-phenylbenzamide (54): A mixture of compound **55** (0.40 g, 1.7 mmol) and Pd/C (10%, 0.08 g) in MeOH and EtOAc (2:1, 15 mL) was hydrogenated and stirred at RT overnight. The reaction mixture was filtered through Celite 545 and washed with MeOH. The filtrate was dried (Na_2SO_4), filtered and evaporated in vacuo to give a yellowish–brown crude solid. This was recrystallized from a mixture of *n*-hexane and THF (2:1) to give a brown solid (compound **54**; 0.13 g, 59% yield). ^{1}H NMR (300 MHz, [D$_6$]DMSO): δ = 9.75 (br s, 1H), 7.76–7.70 (m, 4H), 7.30 (t, 2H, J = 7.9 Hz), 7.03 (t, 1H, J = 7.4 Hz), 6.60 (d, 2H, J = 8.6 Hz), 5.75 (br s, 2H); ^{13}C NMR (75 MHz, [D$_6$]DMSO): δ = 165.3 152.1, 139.8, 129.3, 128.4, 122.9, 121.1, 120.1, 112.5 ppm; LC–MS (212.09) *m/z* 213.0 $[M+H]^+$, 235.0 $[M+Na]^+$; t_R = 14.5 min, purity 95% (method A).

4-Nitro-*N*-phenylbenzamide (55): 4-Nitrobenzoyl chloride (0.20 g, 1.1 mmol, 1.1 equiv) was slowly added to a stirred solution of aniline (0.093 g, 1.0 mmol) and DMAP (6.4 mg, 0.05 mmol, 0.05 equiv) in THF (10 mL) at 0 °C. The resulting solution was allowed to warm to RT and stirred at RT for 6 h. A saturated $NaHCO_3$ solution (3 mL) was added to the reaction mixture, and the resulting mixture was extracted with EtOAc (3×10 mL). The combined organic layers were dried (Na_2SO_4), filtered and evaporated in vacuo to give the crude product as a yellowish brown solid. The solid was recrystallized from a mixture of *n*-hexane and EtOAc (2:1) to give a pale-yellow solid (compound **55**; 0.58 g, 71% yield). ^{1}H NMR (300 MHz, [D$_6$]DMSO): δ = 10.56 (br s, 1H), 8.45–8.26 (m, 2H), 8.23–7.97 (m, 2H), 7.78 (d, J = 8.4 Hz, 2H), 7.38 (t, J = 7.9 Hz, 2H), 7.14 ppm (ddd, J = 7.1, 2.2, 1.1 Hz, 1H); ^{13}C NMR (75 MHz, [D$_6$]DMSO): δ = 163.9, 156.7, 140.5, 139.8, 129.3, 128.7, 124.2, 123.5, 120.5 ppm; LC–MS (242.07) *m/z* 243.1 $[M+H]^+$, 265.0 $[M+Na]^+$; t_R = 21.7 min, purity 96% (method A).

Biochemical and cellular assays

Recombinant ALK catalytic domain was expressed in the *Baculovirus* system, purified by affinity chromatography and used in an ELISA-based kinase assay as described previously.[42] Dose–response curves were generated by plotting normalized kinase activity versus inhibitor concentration. IC_{50} values represent the concentration that causes 50% inhibition relative to the vehicle-treated control samples. Cell growth assays were performed according to the [^{3}H]thymidine incorporation method. Murine IL3-dependent BaF3 cells (control) and NPM–ALK-transfected BaF3 cells[43] were seeded in 96-well plates and incubated with inhibitors for 72 h. An eight-hour [^{3}H]thymidine pulse before harvesting allowed direct measure of the proliferation rate by liquid scintillation. Dose–response curves were obtained, and IC_{50} values were calculated. Every inhibi-

tor was tested at least three times, and each data point was performed in triplicate.

Acknowledgements

We thank Matti Wahlsten and Miikka Olin for technical support. This work was supported by grants from the European Commission (research project no. 503467), the Academy of Finland (research project no. 108376), and the Italian Association for Cancer Research (research project no. IG 10092).

Keywords: anaplastic lymphoma kinase · antitumor agents · inhibitors · medicinal chemistry · structure–activity relationships

[1] R. Chiarle, C. Voena, C. Ambrogio, R. Piva, G. Inghirami, *Nat. Rev. Cancer* **2008**, *8*, 11 – 23.
[2] M. Shiota, J. Fujimoto, T. Semba, H. Satoh, T. Yamamoto, S. Mori, *Oncogene* **1994**, *9*, 1567 – 1574.
[3] T. Iwahara, J. Fujimoto, D. Wen, R. Cupples, N. Bucay, T. Arakawa, S. Mori, B. Ratzkin, T. Yamamoto, *Oncogene* **1997**, *14*, 439 – 449.
[4] U. Kristoffersson, S. Heim, J. Heldrup, M. Åkerman, S. Garwicz, F. Mitelman, *Hereditas* **1985**, *103*, 77 – 84.
[5] R. Morgan, B. K. Hecht, A. A. Sandberg, F. Hecht, S. D. Smith, *N. Engl. J. Med.* **1986**, *314*, 1322.
[6] H. G. Drexler, S. M. Gignac, R. von Wasielewski, M. Werner, W. G. Dirks, *Leukemia* **2000**, *14*, 1533 – 1559.
[7] R. H. Gunby, E. Sala, C. J. Tartari, M. Puttini, C. Gambacorti-Passerini, L. Mologni, *Anti-Cancer Agents Med. Chem.* **2007**, *7*, 594 – 611.
[8] M. Soda, Y. L. Choi, M. Enomoto, S. Takada, Y. Yamashita, S. Ishikawa, S. Fujiwara, H. Watanabe, K. Kurashina, H. Hatanaka, M. Bando, S. Ohno, Y. Ishikawa, H. Aburatani, T. Niki, Y. Sohara, Y. Sugiyama, H. Mano, *Nature* **2007**, *448*, 561 – 566.
[9] E. Lin, L. Li, Y. Guan, R. Soriano, C. S. Rivers, S. Mohan, A. Pandita, J. Tang, Z. Modrusan, *Mol. Cancer Res.* **2009**, *7*, 1466 – 1476.
[10] K. Pulford, S. W. Morris, F. Turturro, *J. Cell. Physiol.* **2004**, *199*, 330 – 358.
[11] K. Pulford, L. Lamant, S. W. Morris, L. H. Butler, K. M. Wood, D. Stroud, G. Delsol, D. Y. Mason, *Blood* **1997**, *89*, 1394 – 1404.
[12] J. G. Bilsland, A. Wheeldon, A. Mead, P. Znamenskiy, S. Almond, K. A. Waters, M. Thakur, V. Beaumont, T. P. Bonnert, R. Heavens, P. Whiting, G. McAllister, I. Munoz-Sanjuan, *Neuropsychopharmacology* **2008**, *33*, 685 – 700.
[13] H. Y. Zou, Q. Li, J. H. Lee, M. E. Arango, S. R. McDonnell, S. Yamazaki, T. B. Koudriakova, G. Alton, J. J. Cui, P. P. Kung, M. D. Nambu, G. Los, S. L. Bender, B. Mroczkowski, J. G. Christensen, *Cancer Res.* **2007**, *67*, 4408 – 4417.
[14] R. Li, S. W. Morris, *Med. Res. Rev.* **2008**, *28*, 372 – 412.
[15] M. E. Noble, J. A. Endicott, L. N. Johnson, *Science* **2004**, *303*, 1800 – 1805.
[16] M. Getlik, C. Grutter, J. R. Simard, S. Kluter, M. Rabiller, H. B. Rode, A. Robubi, D. Rauh, *J. Med. Chem.* **2009**, *52*, 3915 – 3926.
[17] I. Plaza-Menacho, L. Mologni, E. Sala, C. Gambacorti-Passerini, A. I. Magee, T. P. Links, R. M. Hofstra, D. Barford, C. M. Isacke, *J. Biol. Chem.* **2007**, *282*, 29230 – 29240.
[18] A. V. Galkin, J. S. Melnick, S. Kim, T. L. Hood, N. Li, L. Li, G. Xia, R. Steensma, G. Chopiuk, J. Jiang, Y. Wan, P. Ding, Y. Liu, F. Sun, P. G. Schultz, N. S. Gray, M. Warmuth, *Proc. Natl. Acad. Sci. USA* **2007**, *104*, 270 – 275.
[19] C. Pargellis, L. Tong, L. Churchill, P. F. Cirillo, T. Gilmore, A. G. Graham, P. M. Grob, E. R. Hickey, N. Moss, S. Pav, J. Regan, *Nat. Struct. Biol.* **2002**, *9*, 268 – 272.
[20] J. R. Simard, M. Getlik, C. Grutter, V. Pawar, S. Wulfert, M. Rabiller, D. Rauh, *J. Am. Chem. Soc.* **2009**, *131*, 13286 – 13296.
[21] P. T. Wan, M. J. Garnett, S. M. Roe, S. Lee, D. Niculescu-Duvaz, V. M. Good, C. M. Jones, C. J. Marshall, C. J. Springer, D. Barford, R. Marais, *Cell* **2004**, *116*, 855 – 867.
[22] R. T. Bossi, M. B. Saccardo, E. Ardini, M. Menichincheri, L. Rusconi, P. Magnaghi, P. Orsini, N. Avanzi, A. L. Borgia, M. Nesi, T. Bandiera, G. Fogliatto, J. A. Bertrand, *Biochemistry* **2010**, *49*, 6813 – 6825.
[23] C. C. Lee, Y. Jia, N. Li, X. Sun, K. Ng, E. Ambing, M. Y. Gao, S. Hua, C. Chen, S. Kim, P. Y. Michellys, S. A. Lesley, J. Harris, G. Spraggon, *Biochem. J.* **2010**, *430*, 425 – 437.
[24] J. J. Irwin, B. K. Shoichet, *J. Chem. Inf. Model.* **2005**, *45*, 177 – 182.
[25] H. Q. Li, P. C. Lv, T. Yan, H. L. Zhu, *Anti-Cancer Agents Med. Chem.* **2009**, *9*, 471 – 480.
[26] A. Majhi, G. M. Rahman, S. Panchal, J. Das, *Bioorg. Med. Chem.* **2010**, *18*, 1591 – 1598.
[27] M. R. Lee, C. Dominguez, *Curr. Med. Chem.* **2005**, *12*, 2979 – 2994.
[28] L. A. O'Neill, *Nat. Rev. Drug Discovery* **2006**, *5*, 549 – 563.
[29] M. C. Genovese, *Arthritis Rheum.* **2009**, *60*, 317 – 320.
[30] H. Sano, T. Noguchi, A. Tanatani, Y. Hashimoto, H. Miyachi, *Bioorg. Med. Chem.* **2005**, *13*, 3079 – 3091.
[31] R. J. Rahaim, Jr., R. E. Maleczka, Jr., *Org. Lett.* **2005**, *7*, 5087 – 5090.
[32] R. Y. Bai, P. Dieter, C. Peschel, S. W. Morris, J. Duyster, *Mol. Cell. Biol.* **1998**, *18*, 6951 – 6961.
[33] E. Boutet, D. Lieberherr, M. Tognolli, M. Schneider, A. Bairoch, *Methods Mol. Biol.* **2007**, *406*, 89 – 112.
[34] S. F. Altschul, T. L. Madden, A. A. Schaffer, J. Zhang, Z. Zhang, W. Miller, D. J. Lipman, *Nucleic Acids Res.* **1997**, *25*, 3389 – 3402.
[35] J. V. Lehtonen, D. J. Still, V. V. Rantanen, J. Ekholm, D. Björklund, Z. Iftikhar, M. Huhtala, S. Repo, A. Jussila, J. Jaakkola, O. Pentikäinen, T. Nyrönen, T. Salminen, M. Gyllenberg, M. S. Johnson, *J. Comput.-Aided Mol. Des.* **2004**, *18*, 401 – 419.
[36] T. D. Schneider, D. N. Mastronarde, *Discrete Appl. Math.* **1996**, *71*, 259 – 268.
[37] M. S. Johnson, J. P. Overington, *J. Mol. Biol.* **1993**, *233*, 716 – 738.
[38] N. Eswar, B. Webb, M. A. Marti-Renom, M. S. Madhusudhan, D. Eramian, M. Y. Shen, U. Pieper, A. Sali, in *Current Protocols in Protein Science* (Eds: J. E. Coligan, B. M. Dunn, D. W. Speicher, P. T. Wingfield), John Wiley & Sons, Hoboken, **2007**, Unit 2.9, pp. 2.9.1 – 2.9.31.
[39] R. A. Laskowski, M. W. MacArthur, D. S. Moss, J. M. Thornton, *J. Appl. Crystallogr.* **1993**, *26*, 283 – 291.
[40] G. Jones, P. Willett, R. C. Glen, A. R. Leach, R. Taylor, *J. Mol. Biol.* **1997**, *267*, 727 – 748.
[41] M. Rarey, B. Kramer, T. Lengauer, G. Klebe, *J. Mol. Biol.* **1996**, *261*, 470 – 489.
[42] L. Mologni, E. Sala, S. Cazzaniga, R. Rostagno, T. Kuoni, M. Puttini, J. Bain, L. Cleris, S. Redaelli, B. Riva, F. Formelli, L. Scapozza, C. Gambacorti-Passerini, *J. Mol. Endocrinol.* **2006**, *37*, 199 – 212.
[43] R. H. Gunby, S. Ahmed, R. Sottocornola, M. Gasser, S. Redaelli, L. Mologni, C. J. Tartari, V. Belloni, C. Gambacorti-Passerini, L. Scapozza, *J. Med. Chem.* **2006**, *49*, 5759 – 5768.

Received: April 1, 2011
Revised: May 22, 2011
Published online on June 30, 2011

